Effects of Particle Size and Substrate Surface Properties on Deposition Dynamics of Inkjet-Printed Colloidal Drops for Printable Photovoltaics Fabrication

S. Biswas

S. Gawande

V. Bromberg

Department of Mechanical Engineering,
Binghamton University,
Binghamton, NY 13902

Y. Sun[1]
Department of Mechanical Engineering,
Binghamton University,
Binghamton, NY 13902;
Department of Mechanical Engineering and
Mechanics,
Drexel University,
Philadelphia, PA 19104
e-mail: ysun@coe.drexel.edu

Using fluorescence microscopy, the inkjet deposition dynamics of monodispersed polystyrene particles in the size range of 0.02–1.1 μm have been studied on glass, Ar plasma cleaned glass, and PDMS coated glass substrates. The results show that the substrate properties play an important role in determining the final dried patterns formed by the colloidal particles. Our observations also reveal that particle size and contact angle formed by the solvent in the dispersion determine how close to the contact line the particles can be deposited. It is found that smaller particles can move closer to the deposited contact line than particles with bigger sizes. This study can serve as a realistic experimental model system for a number of fundamental queries on how the final deposition microstructure depends on the ink formulation and substrate properties. The knowledge obtained here can be explored further to optimize process parameters for the fabrication of hybrid solar cells with improved morphology and device properties.
[DOI: 10.1115/1.4001470]

Keywords: inkjet printing, colloidal drop deposition, substrate surface energy, solar cells

1 Introduction

In the field of flexible electronics, there has been an increasing interest over the last few years in the development of hybrid solar cells on different flexible substrates using two or more inorganic component materials or a polymer-inorganic blend. These light weight devices for solar energy conversion have various attractive advantages over their silicon counterparts such as easy processing, mechanical flexibility, the potential for low-cost fabrication of large areas, and ample possibilities of optoelectronic tuning of their material properties [1–5]. The ease of fabrication via low temperature evaporation and/or solution processing opens up a potentially wide market for devices made of these materials since they can be integrated onto or into other products such as textiles, packages, portable electronic equipments, etc. In this regard, semiconductor quantum dots attracted much research attention for the designing of next generation solar cells with improved electron generation and device efficiencies [6–8]. These quantum dots are unique, compared with bulk semiconductors or organic sensitizers. Quantum dots such as CdSe, CdTe, PbSe, InAs, etc., with their tunable band gaps offer improved light harvesting capability through the design of rainbow solar cells. They also offer the possibility of generating multiple charge carriers under high energy excitations. Now, the real challenge is to capture these photogenerated electrons as quickly as they are generated, and transport them to the electrode surface in an efficient manner. A common strategy to utilize semiconductor quantum dots in solar cells is to couple them with another large bandgap semiconductor such as TiO_2, ZnO, SnO_2, or carbon fullerenes. Intimate intermixing of the two components of such a bulk-heterojunction (BHJ) solar cell ensures efficient dissociation of strongly bound electron-hole pairs that are generated upon illumination and transport of the spatially separated holes and electrons through the respective phases to the electrodes.

For device fabrication by low-cost solution processes, the photoactive quantum dots offer a distinctive advantage. Most of them can be stabilized as colloidal suspensions with a suitable surface functionality and/or solvent formulations [8,9]. In solution processed photovoltaics, most of the optimization efforts are focused on the chemical structure and purity of the materials being used, as well as the nanomorphology of the deposited photoactive layers. There are several reports on the relationship between the nanomorphology of the photoactive layer (BHJ layer) and the performance of the solar cells [10–12]. Apart from the active materials, a large number of variables, including processing techniques, solvents, concentrations, weight ratio of the components, as well as the thermal annealing temperature can dramatically affect the nanoscale structure of the BHJ layer and thereby its photovoltaic performance.

The mechanism by which nanoparticles suspended in liquids self-organize on substrates attracted much attention because of a large number of potential applications [13,14]. It has been observed that the material of the substrates on which drops of aqueous suspensions containing nanoparticles evaporate has a strong effect on the patterns formed by self-organization of nanoparticles [15]. Patterns formed by drops of evaporating suspensions have been divided into two groups: symmetrical rings and uniform deposition patterns. As reported by Deegan et al. [16,17], as long as the contact line of the deposited drop on the substrate is pinned, the higher evaporative flux at the contact line will drive a replenishing radial flow from the center. This flow is responsible for the

[1]Corresponding author.

Contributed by the Solar Energy Division of ASME for publication in the JOURNAL OF SOLAR ENERGY ENGINEERING. Manuscript received September 3, 2009; final manuscript received December 11, 2009; published online May 10, 2010. Assoc. Editor: Ignacio Tobias.

so-called "coffee-ring" pattern left by evaporating drops carrying solute. The contact line pinning that is essential to this process may initially occur due to substrate heterogeneities but subsequently be reinforced as particles "jam" the contact line during the radial flow. However, if no initial pinning of the contact line occurs, the colloidal drop will undergo self-similar evaporation, i.e., the drop imprint radius decreases but the contact angle maintains roughly the same. For such a case, more uniform particle deposition morphology is expected. Deegan et al. [17] also reported about a weak Marangoni-induced flow in their experiments. A Marangoni force manifests itself when there is a gradient in surface tension along a liquid-gas interface—regions of higher surface tension "pull" the liquid along the interface. Since surface tension is a function of temperature, it was reasoned that a nonuniform temperature profile along the drop surface during evaporation would set up corresponding surface tension gradients to drive the flow. A contact line temperature that is higher than that of the drop apex would be set up due to the longer thermal conduction path that the heat flux from the substrate must follow to replenish the latent heat at the surface.

Inkjet printing has already been established as a convenient technique for controlled deposition of solutions or suspensions of functional materials in specific locations on a substrate, and can be used as a fast deposition technique of photovoltaic films over a large area [18–20]. The main advantage of inkjet printing over other commonly used deposition techniques (e.g., spin coating, spray deposition, dip coating, etc.) is its ability to precisely produce droplets with a consistent volume. Due to this highly controlled deposition feature, the process has been extensively exploited in the field of polymer light emitting diodes and thin film transistors [18,21,22].

Our current research interests are concentrated on studying the inkjet deposition dynamics of colloidal suspensions on various types of flexible substrates such as PET, glass, etc. Model suspension systems consisting of florescent polystyrene particles in aqueous solution are used to obtain real time images of particle deposition in an evaporating drop. Results herein are expected to remain general and can be further expanded for inkjet deposition of solution processed quantum dots and nanocrystals for the fabrication of printable photovoltaic cells. In this paper, the effects of particle size and substrate surface properties on the deposition dynamics of colloidal suspensions are examined using fluorescence microscopy. Aqueous droplets of surface functionalized polystyrene nano/microspheres with sizes ranging from 0.02 μm up to 1.1 μm, are jetted onto glass substrates that have different surface energies, as a result of different surface treatments. The deposition behaviors of these monodispersed colloidal particle dispersions on different glass substrates are discussed in details.

2 Experimental Procedure

2.1 Setup. The custom designed experimental setup used in this study has the facility to visualize the evaporation process and related liquid flows inside a single drop jetted onto a substrate. A schematic of the setup is shown in Fig. 1. A piezoelectric inkjet head with a nozzle diameter of 55 μm (MicroFab Technologies Inc.) was used to generate the drops. A CCD camera coupled with a halogen strobe (Perkin Elmer) was used to measure the diameter and velocity of the drops. Droplet in-flight diameter and velocity control was attained by means of varying the voltage waveform that drives the piezoelectric crystal. During the entire experiment, the droplet in-flight diameter and velocity were maintained to be 50 ± 2 μm and 1.2 ± 0.1 m/s, respectively.

The drops were jetted on microscope glass slides, positioned on the *xy*-stage of a Zeiss Axio Observer A1 inverted fluorescence microscope focused with a 20× objective. The microscope was coupled to a SONY XCL5005CR camera. During jetting, the image acquisition software of the camera continuously scanned the field of view and captured the images. Post-processing of the captured images was done using ImageJ software.

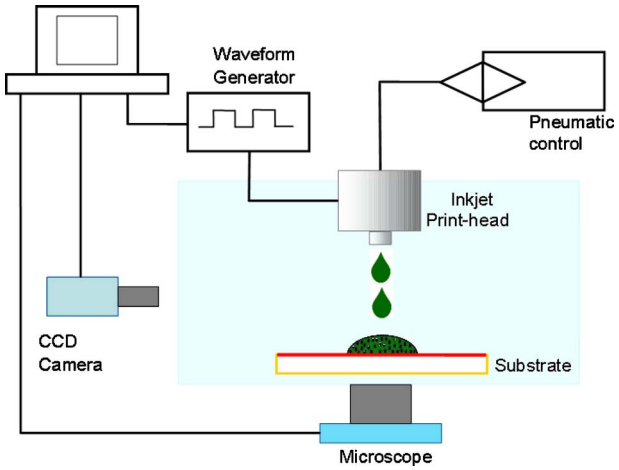

Fig. 1 The ink jet setup

2.2 Materials used. Three batches of monodispersed polystyrene nano/microspheres with a polydispersity less than 3% were obtained from Molecular Probes (Invitrogen, USA). The polystyrene particles had carboxylate surface groups and diameters of 0.02 μm, 0.2 μm, and 1.1 μm, respectively. All the colloidal suspensions were diluted with deionized water to 0.05% prior to deposition to minimize particle effects on the drop. The final dispersion was sonicated to minimize particle aggregation and settling. The substrates used were Corning No.1 cover slips of 130–160 μm thickness (Bellco). The glass slides were thoroughly cleaned by first washing with acetone then deionized water and finally dried using a stream of nitrogen gas. These glass substrates showed water contact angle values of 36 deg (advancing contact angle θ_A) and 17 deg (receding contact angle θ_R). Hydrophobic glass substrates were prepared by coating glass slides with a thin layer of *poly*-dimethylsiloxane (PDMS), which decreases the surface energy; the measured values of water contact angles were $\theta_A = 111$ deg and $\theta_R = 89$ deg. Hydrophilic glass substrates were prepared by treating the glass slides in a low energy Ar plasma etcher (Harrick Plasma) for 15 min, which increases the surface energy of the glass; the water contact angles were $\theta_A = 13$ deg and $\theta_R = 6$ deg.

3 Results and Discussion

A series of experiments were performed with different combinations of monodispersed suspensions and glass substrates to study how colloidal particles interact with the contact line as the drop evaporates. The ambient air temperature is maintained at approximately 24 °C, the relative humidity is about 25%, and jetting parameters (e.g., drop velocity and volume) are maintained to be approximately the same for all the experiments. Analysis of the recorded image sequences, starting from the impact with the substrate and subsequent evaporation of a single jetted drop, reveals the nature of fluid flow inside the drop.

Dimensionless groups that are important in the drop dynamics include the Reynolds number $\mathrm{Re} = UD/\nu$, Weber number $\mathrm{We} = \rho D U^2/\sigma$, and Ohnesorge number $\mathrm{Oh} = \mu/(\rho\sigma D)^{1/2} = (\mathrm{We})^{1/2}/\mathrm{Re}$, where U is the impact speed of the drop, D is the drop diameter, ν and μ are the kinematic and dynamic viscosities of the liquid drop respectively, σ is the interface tension between liquid and vapor, and ρ is the liquid density. Using the drop jetting velocity of 1.2 ± 0.1 m/s and drop diameter of 50 ± 2 μm, it follows that $\mathrm{We} \sim 1$, $\mathrm{Re} \sim 60$, $\mathrm{Oh} \sim 0.017$, and the Bond number defined as $\mathrm{Bo} = \rho g D^2/\sigma$ is very small, such that gravitational effects are negligible. The dimensionless parameter analysis implies that drop spreading is primarily capillary driven.

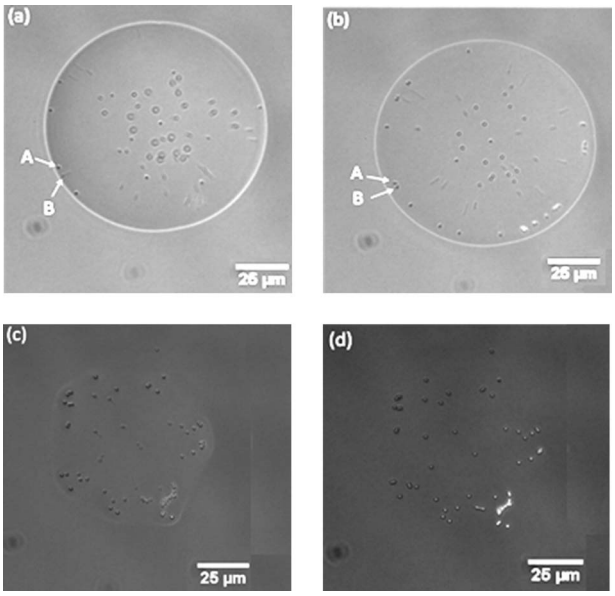

Fig. 2 Sequence of frames recorded after the impact of a jetted drop containing 1.1 μm particles on an Ar plasma treated glass substrate, (*a*) just after the impact, $t=0$ s, (*b*) $t=0.28$ s, when the contact line diameter reaches its maxima (*c*) $t=0.70$ s, and (*d*) $t=1.20$ s, when the drop is completely dried. The pre-impact in-flight diameter and velocity of the drop were 50 μm and 1.2 m/s.

3.1 Effect of Particle Size on the Deposition of Colloidal Suspensions. Figure 2 shows a sequence of frames recorded, starting from the impact of a drop of suspensions containing 1.1 μm particles on an Ar plasma treated glass substrate. A careful inspection of the deposited drop diameter (contact line) shows that it changes characteristically with the evaporation of the drop. During the initial stage, the contact line diameter increases slightly with time, reaches a maximum value and then monotonically decreases until the drop is dried. Further observations on the image sequences reveal that the few particles (e.g., particles A and B in Figs. 2(*a*) and 2(*b*)), which were near the periphery of the droplet during the initial stage of evaporation are not exactly positioned on the contact line of the solvent. During the entire evaporation process, these particles always remain a distance away from the contact line, but they can move parallel to the contact line and come nearer to each other. During the later stage of evaporation when the contact line diameter is decreasing, the next set of particles move toward these particles and forms the coffee-ring structure. The particle deposition diameter is also observed to be changing with time (with the change in contact line diameter).

Figure 3 shows the change in contact line and particle deposition diameters with the evaporation of two similar drops (deposited with all jetting parameters the same) on an Ar plasma treated glass substrate. As mentioned before, for both drops, the contact line diameter increases slightly during the initial stage after the impact with the substrate (spreading of the drop). The particle deposition diameter is also found to be increasing slightly with the increase in contact line diameter. After reaching the maximum, the contact line diameter starts decreasing with the evaporation of the drop. During this stage, the particle deposition diameter follows this decreasing trend of the contact line and monotonically reduced. However, due to the radial flow toward the contact line, more and more particles are moved toward the ring formed by the deposited particles before the drop is completely dried.

As shown in Fig. 4, similar type of behavior of the contact line and particle deposition diameters during evaporation of the deposited drop is also observed on clean glass substrates with the same

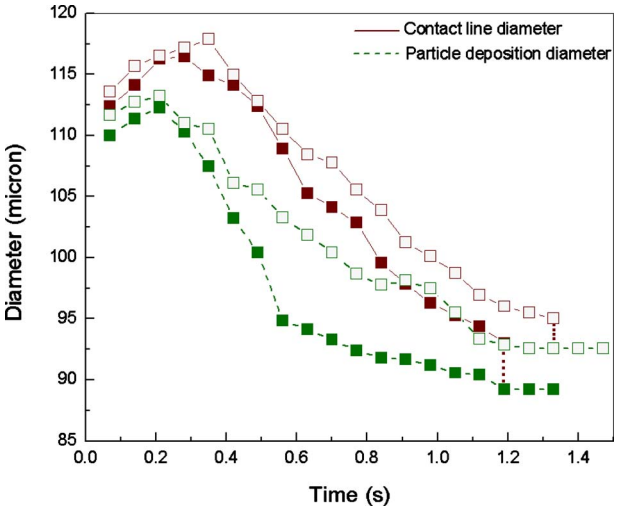

Fig. 3 The change in contact line and particle deposition diameters with the evaporation of two similar drops, containing 1.1 μm particles on an Ar plasma treated glass substrate (filled squares: drop 1 and hollow squares: drop 2)

1.1 μm particle suspensions. The contact line diameter increases slightly after the deposition and then starts decreasing with the evaporation of the drop, whereas, the particle deposition diameter continuously decreases until the drop is completely dried. It is interesting to note that on the clean glass substrates, the change in contact line diameter with time is much larger than the Ar plasma treated substrates.

As suggested by Perelaer et al. [23], the observed difference between the contact line and particle deposition diameters during the evaporation process of a deposited drop of colloidal suspensions can be explained in terms of the contact angle that the solvent forms with the substrate and the size of the particles approaching the contact line. The shape of a droplet edge on a substrate can be approximated to be a triangular wedge with the angle equal to the contact angle. Therefore, the contact angle of the droplet on a substrate limits the deposition of the particles within the droplet. The larger the particles, the greater the distance will be between these particles and the initial contact line. As a result, the diameter of a dried droplet decreases with the increase

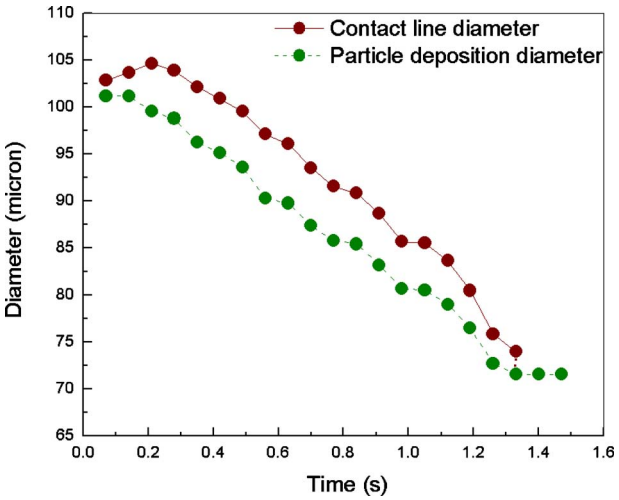

Fig. 4 The change in contact line and particle deposition diameters with the evaporation of a drop containing 1.1 μm particle suspensions on clean glass substrates

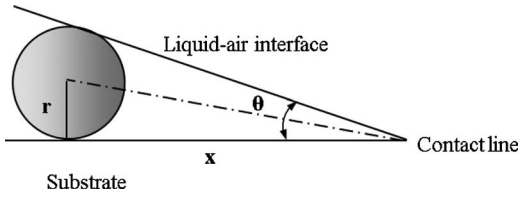

Fig. 5 Schematic representation of the wedge shaped edge of the deposited drop

in particle size (keeping drop volume, velocity, and substrate approximately the same), since larger particles cannot reach as near to the contact line as smaller particles.

As shown in Fig. 5, the distance from a deposited contact line edge particle to the actual contact line can be calculated from a simple tangent equation

$$x = r/\tan(\theta/2) \tag{1}$$

where x represents the distance between the contact line and the center of the particle that is located along the contact line, r is the particle radius, and θ is equal to the contact angle that the solvent forms with the substrate.

Figure 6 shows the measured values of x during evaporation of the two drops (in Fig. 3) on Ar plasma treated glass substrates. Depending on the relative positions of the contact line and deposited particles, the x values first increase and reach a maximum, then start decreasing with the evaporation of the drop. For the 1.1 μm particles, substituting $r=0.55$ μm and $\theta=\theta_A=13$ deg in Eq. (1), yields $x=4.83$ μm. This calculated value is reasonably, the minimum value of x ($x_{\min}$) that could be observed during the initial stage of the evaporation process when the drop is still spreading. However, the observed values of $x_{\min}$ in the two drops are lower than the calculated value. This discrepancy can be attributed to the over simplicity of the model, where it was assumed that the particles are not penetrating outside the liquid envelope, which may not be realistic for a small contact angle.

Figure 7 shows the measured values of x during evaporation of the drop (in Fig. 4) on clean glass substrates. Here, substituting $r=0.55$ μm and $\theta=\theta_A=36$ deg, Eq. (1) yields $x=1.69$ μm. This is reasonably in good agreement with Fig. 7 during the initial stage of evaporation. The above observations suggest that the model represented by Eq. (1), is practically correct for a considerably higher value of the contact angle, however, it fails to predict the value of x when the contact angle is very small.

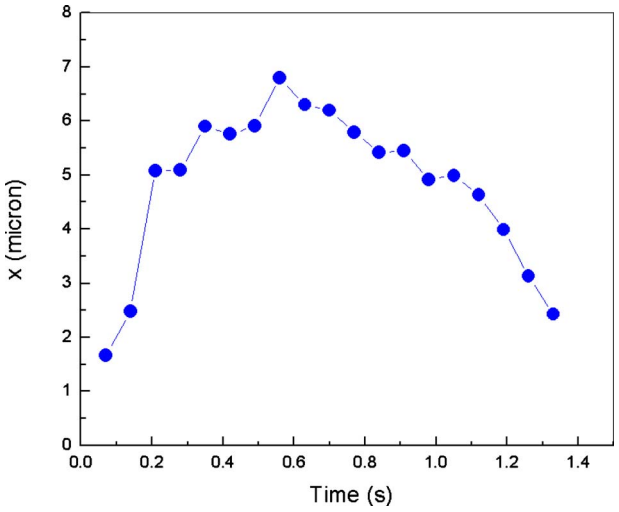

Fig. 7 The values of *x* measured during evaporation of the drop on clean glass substrate in Fig. 4

Figure 8 compares the change in contact line diameter with the evaporation of the deposited droplets of the three types of colloidal suspensions on PDMS coated glass substrates. Irrespective of the particle size, the contact line diameter increases slightly after deposition, then after remaining steady for few moments, abruptly decreases to a much lower value before the drop is dried. The 1.1 μm particles show a smaller diameter of the dried deposited feature on the PDMS coated glass substrates than the smaller particles. The 0.02 μm and 0.2 μm particles show approximately the same value of the dried drop diameter.

3.2 Effect of Substrate Surface Properties on the Deposition of Colloidal Suspensions. To study the effects of substrate surface properties on the deposition of the particles, the three types of aqueous suspensions with different particle sizes were ink jetted (keeping the jetting parameters fixed) on different glass slides, whose surface energy had been modified. Figure 9 shows the average values of the dried droplet diameters observed on different substrates. On the high surface energy Ar treated glass substrates, the 0.02 μm and 0.2 μm particles form the deposited feature with approximately the same diameter (considering the

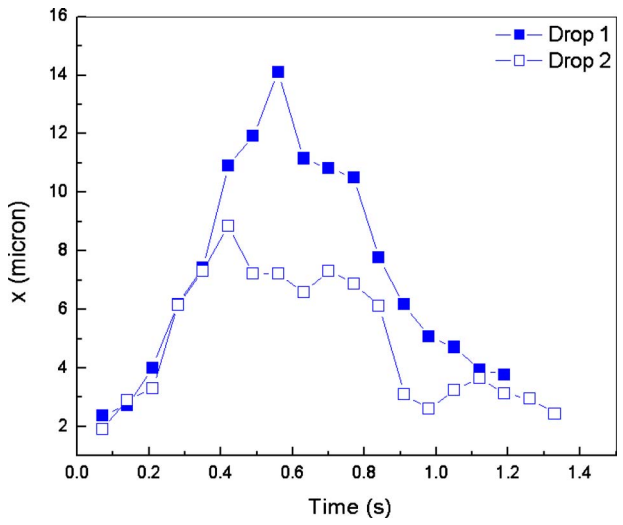

Fig. 6 The measured values of *x* during evaporation of the two drops in Fig. 3

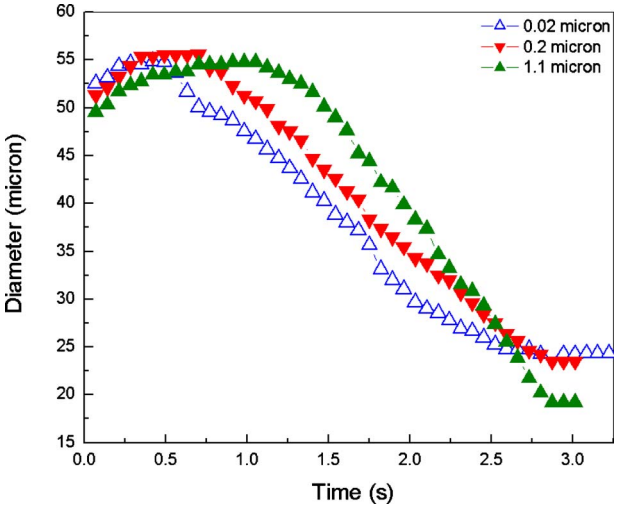

Fig. 8 The variation in contact line diameter with the evaporation of deposited droplets of the three different colloidal suspensions on PDMS coated glass substrates

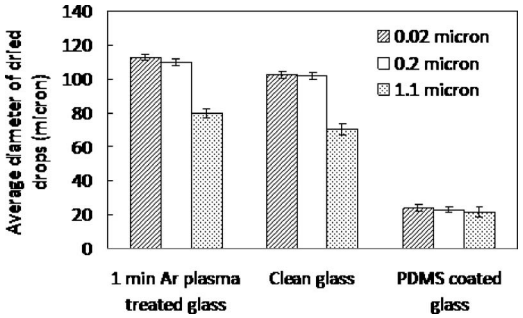

Fig. 9 Average diameter of the deposited dried drops of different particle suspensions on clean glass, Ar plasma treated, and PDMS coated glass substrates

standard deviation of the values). However, the 1.1 μm particles form a much smaller diameter. Similar type of average behavior of the three types of particle suspensions are observed on clean glass samples also.

Figure 10 shows the microscopic images of the dried droplets of the colloidal suspensions on the different substrates, which formed different contact angles with the aqueous solvent. The dashed circles (red) show the maximum diameter position of the contact line after the impact of the droplet with the substrate. From Figs. 9 and 10, it can be concluded that, irrespective of particle size, the diameter of the dried deposited feature decreases with the increase in contact angle. Considering the standard deviation values (as given in Fig. 9), all the particles show approximately the same diameter of the dried deposited feature on the low surface energy PDMS coated glass substrates.

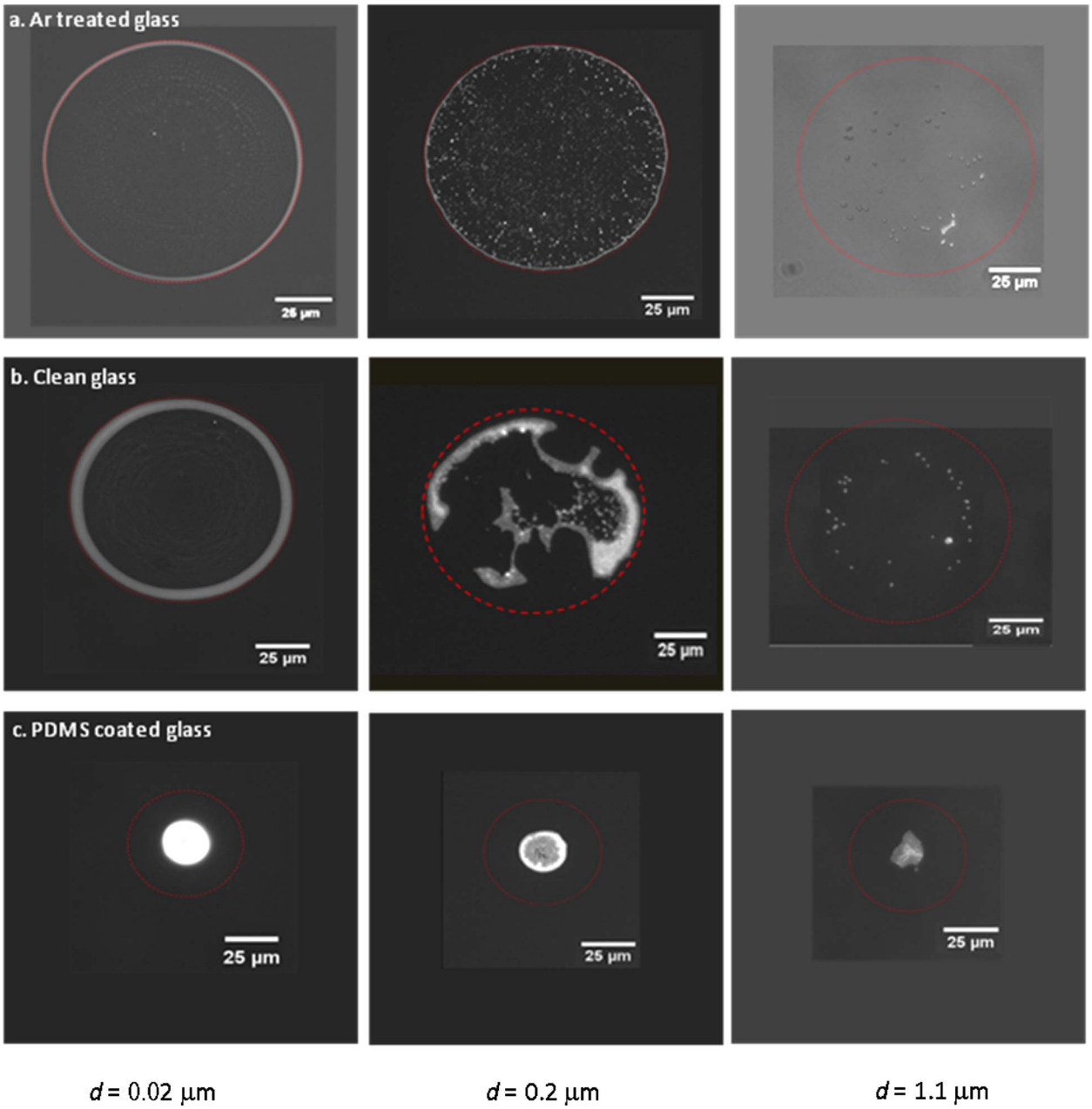

Fig. 10 Microscopic images of inkjet deposited dried droplets of aqueous suspensions of polystyrene particles on (*a*) Ar treated glass, (*b*) clean glass, and (*c*) PDMS coated glass substrates. Each row, from left to right, shows a particle size of 0.02 μm, 0.2 μm, and 1.1 μm, respectively. The red dashed circles show the maximum diameter position of the contact line with the substrate.

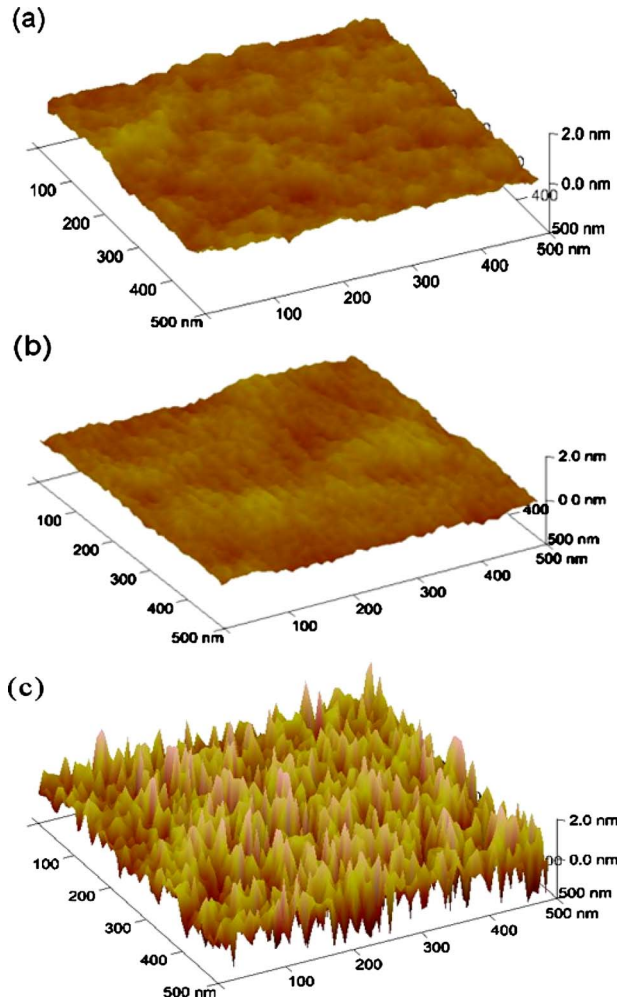

Fig. 11 AFM images of (*a*) clean glass, (*b*) Ar plasma treated, and (*c*) PDMS coated glass samples

Figure 11 compares the AFM images of clean glass, Ar plasma treated and PDMS coated glass substrates. Apart from changing the contact angle, the Ar plasma treatment of the glass substrates increases the nanoscale roughness of the samples. The average roughness value has been increased from 0.407 nm to 0.99 nm after the plasma treatment. As evidently, the increase in roughness has markedly changed the deposition behavior of the colloidal suspensions. For all three types of particle sizes, the diameter of the dried deposited feature is increased after the plasma treatment. On the other hand, the PDMS surface is characteristically very rough (average roughness=3.12 nm).

Figure 12 compares the variation in contact line diameter with evaporation of an ink jetted droplet containing 0.2 μm particles on Ar plasma treated and clean glass substrates. On both types of substrates, the contact line diameter first increases and reaches a steady value, and then decreases before the drop is completely dried. This decrease in contact line diameter during the later stage of evaporation is reasonably due to the depinning of the drop. Similar type of behavior of the drop on clean glass substrates is also observed with the 0.02 μm particles (Fig. 13). However, the 0.02 μm particles on Ar treated glass substrates show an increasing diameter of the contact line before reaching a steady value.

Our studies reveal that substrate surface properties, primarily roughness and hydrophobicity, control the final patterns formed by the self-assembly of the particles in the deposited drops. It is also disclosed that as the size decreases, the particles are more and more preferentially deposited near the contact line. These fundamental observations on the depositions of droplets of suspensions containing nanoparticles on substrates of varying degrees of wetabilities are particularly important for understanding the inkjet deposition behavior of actual inks containing metallic nanoparticles for the fabrication of device structures. Through these in situ studies with the model system of fluorescent polystyrene particles, we have highlighted on the deposition behavior of suspensions of particle sizes down to 20 nm. Further studies of colloidal drop deposition dynamics for printable photovoltaic fabrication, including the deposition of the photoactive layer (e.g., quantum dots) and silver contact lines and bus lines, are being performed to optimize substrate and ink properties, as well as process parameters, for the fabrication of hybrid solar cells with improved morphology and device properties.

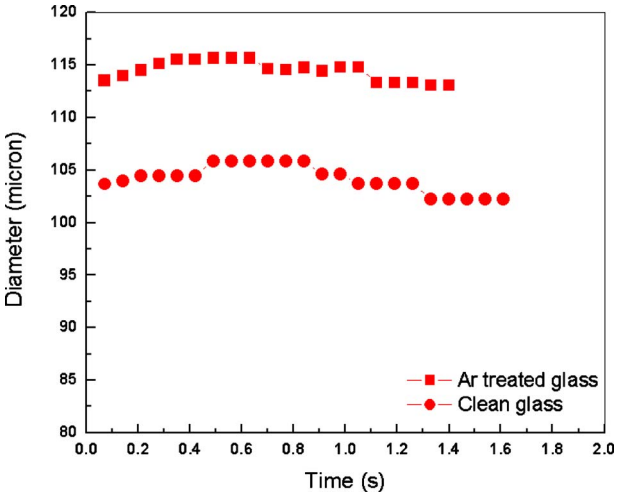

Fig. 12 The variation in contact line diameter with the evaporation of a deposited droplet containing 0.2 μm particles on Ar plasma treated and clean glass substrates

4 Summary

The effects of particle size and substrate surface properties on the deposition dynamics of colloidal suspensions have been studied by ink jetting monodispersed polystyrene particles of sizes 0.02 μm, 0.2 μm, and 1.1 μm on three types of glass substrates having different surface energies. The preferential deposition of

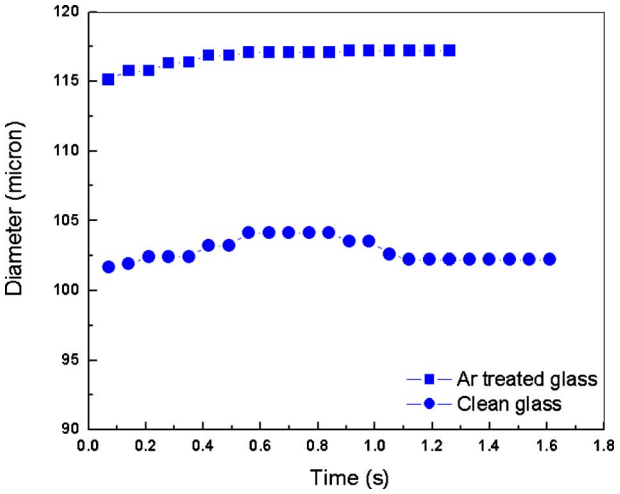

Fig. 13 The variation in contact line diameter with the evaporation of a deposited droplet containing 0.02 μm particles on Ar plasma treated and clean glass substrates

particles near the contact line depending on the particle size and the contact angle formed by solvent in the dispersion is highlighted in this study. We observe that substrate surface properties, including nanoscale roughness and hydrophobicity, have a decisive role on the morphology of the final deposits. It is found that the diameter of the dried deposited features decrease with the increase in hydrophobicity of the substrates, irrespective of particle sizes. On Ar plasma treated glass ($\theta_A = 13$ deg), the smaller particles (0.02 μm and 0.2 μm) show larger depositions than the bigger 1.1 μm particles. A similar type of behavior of the dried deposited features are also observed on clean glass samples ($\theta_A = 36$ deg). In contrast, on PDMS, coated glass ($\theta_A = 111$ deg), the behavior of the contact line diameter with the evaporation of the drop is similar for all types of particles. On an average, the diameters of the dried deposited features on PDMS coated glass substrates are independent of particle sizes.

Acknowledgment

The authors would like to thank the National Science Foundation (Grant No. 0846825) and Center for Advanced Microelectronics Manufacturing (CAMM) at the State University of New York at Binghamton for providing financial support.

Nomenclature

Bo = Bond number
D = drop diameter
g = gravitational acceleration rate
Oh = Ohnesorge number
r = particle radius
Re = Reynolds number
U = impact speed of drop
We = Weber number
x = distance between contact line and center of the particle along the contact line

Greek Symbols

μ = dynamic viscosity
ν = kinematic viscosity
θ = contact angle
ρ = liquid density
σ = surface tension

Subscripts

A = advancing
R = receding

References

[1] Brabec, C. J., Shaheen, S. E., Winder, C., Sariciftci, N. S., and Denk, P., 2002, "Effect of LiF/Metal Electrodes on the Performance of Plastic Solar Cells," Appl. Phys. Lett., **80**(7), pp. 1288–1290.
[2] Al-Ibrahim, M., Ambacher, O., Sensfuss, S., and Gobsch, G., 2005, "Effects of Solvent and Annealing on the Improved Performance of Solar Cells Based on Poly(3-Hexylthiophene): Fullerene," Appl. Phys. Lett., **86**, p. 201120.
[3] Mayer, A. C., Scully, S. R., Hardin, B. E., Rowell, M. W., and McGehee, M. D., 2007, "Polymer-Based Solar Cells," Mater. Today, **10**(11), pp. 28–33.
[4] Hadipour, A., de Boer, B., and Blom, P. W. M., 2007, "Solution-Processed Organic Tandem Solar Cells With Embedded Optical Spacers," J. Appl. Phys., **102**, p. 074506.
[5] Moet, D. J. D., Koster, L. J. A., de Boer, B., and Blom, P. W. M., 2007, "Hybrid Polymer Solar Cells From Highly Reactive Diethylzinc: MDMO–PPV Versus P3HT," Chem. Mater., **19**(24), pp. 5856–5861.
[6] Franceschetti, A., An, J. M., and Zunger, A., 2006, "Impact Ionization Can Explain Carrier Multiplication in PbSe Quantum Dots," Nano Lett., **6**(10), pp. 2191–2195.
[7] Kamat, P. V., 2007, "Meeting the Clean Energy Demand: Nanostructure Architectures for Solar Energy Conversion," J. Phys. Chem. C, **111**(7), pp. 2834–2860.
[8] Brown, P., and Kamat, P. V., 2008, "Quantum Dot Solar Cells. Electrophoretic Deposition of CdSe–C_{60} Composite Films and Capture of Photogenerated Electrons With nC_{60} Cluster Shell," J. Am. Chem. Soc., **130**(28), pp. 8890–8891.
[9] Peng, Z. A., and Peng, X., 2001, "Formation of High-Quality CdTe, CdSe, and CdS Nanocrystals Using CdO as Precursor," J. Am. Chem. Soc., **123**(1), pp. 183–184.
[10] Shaheen, S. E., Brabec, C. J., Sariciftci, N. S., Padinger, F., Fromherz, F., and Hummelen, J. C., 2001, "2.5% Efficient Organic Plastic Solar Cells," Appl. Phys. Lett., **78**, pp. 841–843.
[11] Martens, T., Haen, J. D., Munters, T., Beelen, Z., Goris, L., Manca, J., Olieslaeger, M. D., Vanderzande, D., Schepper, L. D., and Andriessen, R., 2003, "Kelvin Probe Force Microscopy Study on Conjugated Polymer/Fullerene Bulk Heterojunction Organic Solar Cells," Synth. Met., **138**, pp. 243–247.
[12] Hoppe, H., and Sariciftci, N. S., 2004, "Organic Solar Cells: An Overview," J. Mater. Res., **19**, pp. 1924–1945.
[13] Magdassi, S., Grouchko, M., Toker, D., Kamyshny, A., Balberg, I., and Millo, O., 2005, "Ring Stain Effect at Room Temperature in Silver Nanoparticles Yields High Electrical Conductivity," Langmuir, **21**, pp. 10264–10267.
[14] de Gans, B.-J., Hoeppener, S., and Schubert, U. S., 2006, "Polymer-Relief Microstructures by Inkjet Etching," Adv. Mater., **18**, pp. 910–914.
[15] Sommer, A. P., 2004, "Limits of the Impacts of Gravity on Self-Organizing Nanospheres," J. Phys. Chem. B, **108**(24), pp. 8096–8098.
[16] Deegan, R. D., Bakajin, O., Dupont, T. F., Huber, G., Nagel, S. R., and Witten, T. A., 1997, "Capillary Flow as the Cause of Ring Stains From Dried Liquid Drops," Nature (London), **389**, pp. 827–829.
[17] Deegan, R. D., Bakajin, O., Dupont, T. F., Huber, G., Nagel, S. R., and Witten, T. A., 2000, "Contact Line Deposits in an Evaporating Drop," Phys. Rev. E, **62**, pp. 756–765.
[18] Bharathan, J., and Yang, Y., 1998, "Polymer Electroluminescent Devices Processed by Inkjet Printing: I. Polymer Light-Emitting Logo," Appl. Phys. Lett., **72**, pp. 2660–2663.
[19] Speakman, S. P., Rozenberg, G. G., Clay, K. J., Milne, W. I., Ille, A., Gardner, I. A., Bresler, E., and Steinke, J. H. G., 2001, "High Performance Organic Semiconducting Thin Films: Inkjet Printed Polythiophene [rr-P3HT]," Org. Electron., **2**(2), pp. 65–73.
[20] Fuller, S. B., Wilhelm, E. J., and Jacobson, J. M., 2002, "Inkjet Printed Nanoparticle Microelectromechanical Systems," J. Microelectromech. Syst., **11**(1), pp. 54–60.
[21] Ridley, B. A., Nivi, B., and Jacobson, J. M., 1999, "All-Inorganic Field Effect Transistors Fabricated by Printing," Science, **286**(5440), pp. 746–749.
[22] Sirringhaus, H., Kawase, T., Friend, R. H., Shimoda, T., Inbasekaran, M., Wu, W., and Woo, E. P., 2000, "High-Resolution Inkjet Printing of All-Polymer Transistor Circuits," Science, **290**(5499), pp. 2123–2126.
[23] Perelaer, J., Smith, P. J., Hendriks, C. E., vanden Berg, A. M. J., and Schubert, U. S., 2008, "The Preferential Deposition of Silica Micro-Particles at the Boundary of Inkjet Printed Droplets," Soft Matter, **4**, pp. 1072–1078.